The density of ambient black carbon retrieved by a new method:

implications to CCN prediction

Jingye Ren[1, 2], Fang Zhang[2*], Lu Chen[1], Jieyao Liu[1]

[1]*College of Global Change and Earth System Science, Beijing Normal University, Beijing 100875, China*

[2]*Shenzhen Key Laboratory of Organic Pollution Prevention and Control, School of Civil and Environmental Engineering, Harbin Institute of Technology (Shenzhen), 518055 Shenzhen, China*

*Correspondence to: **Fang Zhang (zhangfang2021@hit.edu.cn)**

Abstract.

The effective density of black carbon (BC) is a crucial factor relevant to its aging degree that would add uncertainty in evaluating its climate effect. Here, we have developed a new method to retrieve the effective density of internally mixed BC in the atmosphere combining field observations conducted on 15 November -14 December 2016 in urban Beijing with the Köhler theory. The uncertainty of the retrieval method was evaluated within ±30 %, which is primarily caused by assumptions of the hygroscopic parameter of organics and the fraction of primary organic aerosols in non-hygroscopic or hygroscopic mode. Using the method, we obtain that the ambient internally-mixed BC, accounting for 80±20 % of total BC aerosol particles, is retrieved with campaign mean density of 1.1±0.6 g cm^{-3} during the observed periods. The retrieved result is comparable with that reported in the literatures. By applying a lower (0.14 g cm^{-3}) and upper (2.1 g cm^{-3}) limit of the retrieved BC density in cloud condensation nuclei (CCN) number concentrations (N_{CCN}) estimation, we derived that neglect of such variations in BC density led to an uncertainty of -28 %~11 % in predicting N_{CCN} at supersaturations of 0.23 % and 0.40 %. We also find that the N_{CCN} is more sensitive to the variations of BC density when it is <1.0 g cm^{-3}. This illustrates a necessity of accounting for the effect of BC density on CCN activity closer to source regions where the BC particles are mostly freshly emitted. The CCN closure achieves when introducing the retrieved real-time BC density and mixing state. This study provides a unique way of utilizing field measurements to infer ambient BC density and

highlights the importance of applying variable BC density values in models when predicting CCN and assessing its relevant climate effect.

1 Introduction

Black carbon (BC) aerosols, as the major absorber of solar radiation, play a vital role in energy budget and climate of the earth-atmosphere system by affecting the radiative forcing and cloud properties (Flanner et al., 2007; Ramanathan and Carmichael, 2008). The light-absorbing capability induced by BC is related to its density and morphology (Zhang et al., 2008; Rissler et al., 2014), which can be modified after mixing with other atmospheric aerosol particles (Khalizov et al., 2009; Xue et al., 2009). Changes in its physicochemical properties would also regulate its ability to serve as cloud condensation nuclei (CCN) and further indirectly affect the radiative balance by affecting the clouds process (Yuan et al., 2008; Wang et al., 2011). Owing to the complex evolution of the mixing state, density and morphology of BC, the contribution of BC particles to CCN budgets is still not well understood.

BC particles, with diesel vehicles, industrial and residential coal combustion as major sources, are ubiquitous in urban environments (Bond et al., 2013; Dameto et al., 2017; Li et al., 2017; Liu et al., 2019a). The mixing state of BC describes the distribution of the bare BC and coating masteries among the aerosol population. Typically, freshly generated BC exists in the form of chain aggregates and initially uncoated, which is known as externally mixed BC (Ex-BC). When the BC particles were emitted, they generally mix with other materials by condensation, coagulation,

67 and other processes (Riemer et al., 2004; Zhang et al., 2008; Liu et al., 2013; Zhang et

68 al., 2020a), forming the internally mixed BC (In-BC) particles consisting of BC core

69 and other chemical components (Cheng et al., 2006; Zhang et al., 2016). The BC

70 structure would be more compact with regular shapes (Pagels et al., 2009; Zhang et al.,

71 2008; Wang et al., 2017), and the effective density of internally mixed BC are changed

72 accordingly with the reconstruction (Liu et al., 2019b). The density and morphology of

73 BC particles are closely related to its sources, mobility size, coating thickness, coating

74 material and its chemical composition (Zhang et al., 2008; Pagels et al., 2009; Peng et

75 al., 2016; Zhang et al., 2022). A wide range of BC density has been reported in previous

76 studies (Lide 1992; Mcmurry et al., 2002; Park et al., 2004; Kiselev et al., 2010). Recent

77 field measurements have indicated that the average BC density is ~1.2 g cm^{-3} in the

78 ambient atmosphere (Zhang et al., 2016). Field measurements have also indicated that

79 a considerable fraction of externally mixed/uncoated BC exists (Clarke et al., 2004;

80 Cheng et al., 2012), although a higher proportion of internally mixed/aged BC particles

81 in the ambient atmosphere were observed (Schwarz et al., 2008; Massoli et al., 2015;

82 Chen et al., 2020). In climate models, the BC was generally assumed completely

83 internally-mixed and treated to have a void-free spherical structure and a density value

84 of 1.8 g cm^{-3} (Bond et al., 2013). This may lead to bias in estimating the climate effect

85 driven by BC.

86   Previous study based on a case study show that when the aging degree of ambient

87 particles is low, the BC density (~1.8 g cm^{-3}) under the spherical assumption will lead

88 to the overestimation of particle hygroscopicity by 40-50 % and the overestimation can

89   be explained almost 100 % using the effective density of fresh BC (~0.45 g cm^{-3}) (Fan

90   et al. 2020). This indicates the importance of using reasonable BC density values in the

91   calculation of particle hygroscopicity. In addition, when estimating the CCN number

92   concentration, a significant bias of –35 % ~ +20 % was found due to the assumption of

93   particle mixing state (Ren et al., 2018). However, these studies have not yet accounted

94   for such impact of BC density and mixing state on CCN prediction due to lack of real

95   time measurement data.

96   The mixing state and the density of BC particles are usually directly measured by

97   several techniques, such as an integrated system of a volatility tandem differential

98   mobility analyzer and a single particle soot photometer (VTDMA-SP2) (Zhang et al.,

99   2016), or a differential mobility analyzer with a SP2 (DMA-SP2) (Olfert et al., 2007;

100   Rissler et al., 2014; Wu et al., 2019), and a differential mobility analyzer–centrifugal

101   particle analyzer–single-particle soot photometer (DMA–CPMA–SP2) system (Liu et

102   al., 2019b; Yu et al., 2020), etc. However, such techniques or measurements are not

103   available in many previously conducted filed campaigns. In this study, we develop a

104   novel method for retrieving the mixing state and effective density of ambient BC

105   particles by combining field measured hygroscopic growth factor and aerosol chemical

106   composition and Köhler theory (Petters and Kreidenweis, 2007). The uncertainty of the

107   new retrieval method was evaluated. The retrieved results were also compared and

108   validated with existing observations. In addition, the effect of BC density and mixing

109   state on prediction of CCN number concentrations is further evaluated through a

110   sensitivity and closure test by accounting for the retrieved real-time variations of BC

111   density and mixing state.

112   **2 Field measurements and methodology**

113   **2.1 Field measurements**

114   Measurements in this study were conducted from 15 November to 14 December

115   2016 at a typical urban site of Beijing (39.97°N, 116.37°E, 49 m above sea level). The

116   site locates at the Institute of Atmospheric Physics, Chinese Academy of Sciences,

117   which is mainly influenced by the surrounding cooking, road traffic and residential coal

118   burning emissions during the home heating periods (Sun et al., 2016). The detailed

119   information about the sampling site was presented in previous studies (Sun et al., 2015;

120   Zhang et al., 2019). The number concentration of condensation nuclei (CN) at each size

121   was measured by a scanning mobility particle sizer, which is equipped with a

122   differential mobility analyzer (DMA; model 3081, TSI) and a condensation particle

123   counter (CPC; model 3772, TSI). Subsequently, the mono-dispersed particles were

124   introduced into a Droplet Measurement Technologies CCN counter (CCNc, DMT;

125   Lance et al., 2006) to measure CCN number concentration. A hygroscopic tandem

126   differential mobility analyzer (HTDMA) system was used to measure the hygroscopic

127   growth factor (Gf) (Tan er al., 2013). Here, four diameters of 40, 80, 110, 150, and 200

128   nm are selected in the campaign. Gf is defined as the ratio of the mobility diameter at

129   the given RH to the dry diameter (Petters and Kreidenweis, 2007). The nonrefractory

130   submicron aerosol chemical composition was measured by an Aerodyne high-

131   resolution time-of-flight aerosol mass spectrometer (HR-AMS; Xu et al., 2019),

132   including sulfate, nitrate, ammonium, chloride, and organics. Two factors, including a

133   non-hygroscopic primary organic aerosol (POA) and hygroscopic secondary organic

134   aerosol (SOA) were classified by positive matrix factorization (PMF) with PMF

135   algorithm (v4.2) method (Paatero and Tapper, 1994) and followed the procedures

136   reported in Ulbrich et al. (2009). The refractory black carbon mass loading was

137   measured by an aethalometer (model AE33, Magee Scientific Corporation). Both the

138   nonrefractory materials and BC mass concentration were measured with diameters <

139   1.0 μm. The detailed description of the instrument operation and data process have been

140   described in details elsewhere (Ren et al., 2018; Xu et al., 2019; Zhang et al., 2019; Fan

141   et al., 2020).

142   **2.2 Retrieving the mixing state and density of BC**

143   2.2.1 Retrieving the mixing state of BC

144   The Gf probability distribution function (Gf-PDF) for a specified diameter can be

145   retrieved firstly based on the TDMAinv algorithm (Gysel et al., 2009). The κ-PDF can

146   be further calculated based on the Gf-PDF (Fan et al., 2020). Size-resolved κ is derived

147   using κ-Köhler theory based on hygroscopic growth factor (Gf) (Petters and

148   Kreidenweis, 2007),

149   $$\kappa_{gf} = (\text{Gf}^3 - 1) \cdot \left[\frac{1}{\text{RH}} \exp\left(\frac{4\sigma_{s/a} M_w}{RT\rho_w D_d \text{Gf}} \right) - 1 \right] \tag{1}$$

150   where Gf is hygroscopic growth factor, RH is the relative humidity in the HTDMA

151   (90 %), D_d is the dry diameter, $\sigma_{s/a}$ is assumed to be the surface tension of pure water,

152   R is the universal gas constant, T is the temperature, M_w and ρ_w is the molecular mass,

153   and the density of water, respectively.

154   The κ-PDF patterns of particles in different sizes always present two modes: nearly

155   hydrophobic (NH) mode with $\kappa_{gf} \leq 0.1$ and more hygroscopic (MH) mode with $\kappa_{gf} > 0.1$

156   (Fig. S1). Firstly, based on the κ-PDF patterns, the number fraction (NF) of the total

157   nearly hydrophobic group with the boundary of [0, 0.1] was calculated according to the

158   following equation:

159
$$NF = \int_0^{0.1} c(\kappa, D_p)\, d\kappa \tag{2}$$

160   here, the κ-PDF, represented by $c\,(\kappa, D_p)$, was normalized as $\int c(\kappa, D_p)\, d\kappa = 1$, where

161   κ can be replaced by κ_{gf}, D_p is the selected electrical mobility diameter in the campaign.

162   The nearly hydrophobic mode consists of both externally mixed POA (Ex-POA or

163   bare POA) and externally mixed BC (Ex-BC). Since the number fraction of the nearly-

164   hydrophobic POA would change with the emission and aging processes, in this study,

165   we have applied different values for the number fractions of hydrophobic POA (NH-

166   POA) under clean (91 %), moderately polluted (70 %), and heavily polluted conditions

167   (31 %) by referring the literature (Liu et al., 2021a), as shown in Fig. S2. The number

168   concentration of Ex-BC was then calculated using the total number fraction of NH

169   mode minus the number of NH-POA.

170
$$N_{POA-containing} = N_{total} \times NF_{POA-containing}$$

171
$$N_{bare-POA} = N_{POA-containing} \times NF_{bare-POA}$$

172
$$N_{Ex-BC} = N_{NH} - N_{bare-POA} \tag{3}$$

173   where $N_{POA\text{-}containing}$ and $NF_{POA\text{-}containing}$ are the number concentration and fraction of

174   POA-containing particles, N_{total} is the total number concentration, $N_{bare-POA}$ and NF_{bare-}

175    $_{POA}$ are the number concentration and fraction of bare POA particles, and N_{NH} is the

176   number of nearly- hydrophobic group.

177   The number size distribution of the externally mixed BC (n_{Ex-BC} (log D_p)) can be

178   calculated based on the particle number size distribution (PNSD) and the number

179   fraction of the hydrophobic mode of BC (NF_{Ex-BC}) as follows:

180                         $$n_{Ex-BC}(\log Dp) = NF_{Ex-BC} \times n\,(\log Dp)$$ (4)

181   where n (log D_p) is the function of the aerosol number size distribution, D_p is the

182   mobility diameter.

183   By assuming that the particles are spherical (Rader and McMurry, 1986), the mass

184   size distribution of Ex-BC (M_{Ex-BC}) was obtained as follows:

185                         $$M_{Ex-BC}(\log Dp) = \frac{\pi}{6} D_p{}^3 \rho n_{Ex-BC}(\log Dp)$$ (5)

186   where D_p is the mobility diameter, ρ is the effective density of Ex-BC, and n_{Ex-BC} (log

187   D_p) is the function of the number size distribution of Ex-BC, respectively. By reviewing

188   and summarizing the existing results about, we show that typical values of density for

189   the freshly emitted or externally mixed BC observed in the winter of urban Beijing or

190   North China Plain spans over 0.14-0.50 g cm^{-3}, with mean of ~0.40±0.10 g cm^{-3} (Fig.

191   S3), in the size range of 100 to 300 nm, where the mass concentration of externally

192   mixed BC accounted for a large proportion in urban Beijing (Geller et al., 2006; Peng

193   et al., 2016, 2017; Wu et al., 2019; Liu et al., 2020; Zhao et al., 2022). Therefore, an

194   average ρ_{Ex-BC} of 0.4 g cm^{-3} was used for calculating the mass concentration of

195   externally-mixed BC in our study. The uncertainty analysis exhibits that the variations

196 of the $\rho_{\text{Ex-BC}}$ could lead to an average deviation of ±10 % in the calculating In-BC

197 density (Fig. 3e) by increasing the $\rho_{\text{Ex-BC}}$ from 0.1 to 0.6 g cm^{-3}, showing a small impact

198 on the retrieved result. Uncertainty analyses due to the variations of $\rho_{\text{Ex-BC}}$ were given

199 in section 2.3.

200 The mass size distribution of Ex-BC was fit using the log-normal distribution as

201 shown in Fig. S4 (Wu et al., 2017; Liu et al., 2019a; Zhao et al., 2022). Thus, the bulk

202 mass concentration of Ex-BC can be calculated from the integration of the mass size

203 distribution:

$$m_{\text{Ex-BC}} = \int_{D_{start}}^{D_{end}} M_{\text{Ex-BC}}(\log D_p) \, d \log(D_p) \tag{6}$$

$$m_{\text{In-BC}} = m_{\text{BC}} - m_{\text{Ex-BC}} \tag{7}$$

206 where D_{start} and D_{end} are the lower and upper size limit, $M_{\text{Ex-BC}}$ ($\log D_{\text{p}}$) is the function

207 of the Ex-BC mass size distribution. We then obtained the bulk mass concentration of

208 internally mixed BC ($m_{\text{In-BC}}$) by subtracting $m_{\text{Ex-BC}}$ from the bulk BC mass

209 concentration measured by AE33 in equation 7.

210 2.2.2 Retrieving the density of BC

211 For retrieval of the density of BC, the principal idea is to use the measured κ_{gf} to

212 calculate the density of BC based on the Zdanovskii–Stokes–Robinson (ZSR) mixing

213 rule (Stokes and Robinson, 1966; Zdanovskii, 1948) with the chemical composition

214 measured by AMS (Petters & Kreidenweis, 2007). In the retrieval, several aspects are

215 concerned. First, since the ZSR rule is to assume the aerosol particles are internally

216 mixed, the κ_{gf} value of the more MH mode ($\kappa_{\text{gf-MH}}$) is thus applied for retrieving the

217 density of internally mixed BC. Second, since the size distribution of BC number

218 concentration is usually with peaks between 100 and 200 nm (Liu et al., 2019a; Yu et

219 al., 2020; Zhao et al., 2022), the $\kappa_{\text{gf-MH}}$ value of particles in accumulation mode was

220 averaged and applied for the retrieval. Previous studies showed an independence of $\kappa_{\text{gf-}}$

221 $_{\text{MH}}$ on particle size when the D_p >100 nm during the campaign period (Fan et al., 2020).

222 Therefore, the average of $\kappa_{\text{gf-MH}}$ in accumulation mode is reasonable for the

223 determination of the In-BC density. In addition, because the inversion including

224 measurements from HTDMA and HR-AMS, a total mass closure of the measured

225 aerosol particles was conducted between the two techniques by comparing the mass

226 concentration of PM$_1$ and the results are well consistent (Fig. S5). The density of

227 internally mixed BC (In-BC), $\rho_{\text{In-BC}}$ is then derived from the following equations:

228 $$\kappa_{gf-MH} = \kappa_{chem} = \sum_i \varepsilon_i \kappa_i = \frac{v_{inorg}}{v_{total}} \kappa_{inorg} + \frac{v_{SOA}}{v_{total}} \kappa_{SOA} + \frac{v_{In-POA}}{v_{total}} \kappa_{POA} + \frac{v_{In-BC}}{v_{total}} \kappa_{BC} \qquad (8)$$

229 where $\kappa_{\text{gf-MH}}$ is the hygroscopic parameter of the more hygroscopic (MH) mode, κ_{chem}

230 is the hygroscopic parameter of aerosol particles in the mixed composition and can be

231 calculated based on chemical volume fractions using a simple rule (Stokes and

232 Robinson, 1966; Petters & Kreidenweis, 2007), κ_i is the hygroscopic parameter of each

233 pure composition and ε_i is the volume faction of the individual components in the

234 internal-mixed particle. v_{inorg}, v_{SOA} and $v_{\text{In-POA}}$ are the volume of the inorganic, SOA

235 and internally mixed POA species, and can be calculated as follows: $v_{inorg} = \frac{m_{inorg}}{\rho_{inorg}}$,

236 $v_{SOA} = \frac{m_{SOA}}{\rho_{SOA}}$, and $v_{In-POA} = \frac{m_{In-POA}}{\rho_{POA}}$. v_{total} is the total volume of all the species and can be

237 written as $v_{total} = \frac{m_{inorg}}{\rho_{inorg}} + \frac{m_{SOA}}{\rho_{SOA}} + \frac{m_{In-POA}}{\rho_{POA}} + \frac{m_{In-BC}}{\rho_{In-BC}}$. In equation (8), κ_{BC} and κ_{POA} are

238 assumed to be 0. Then, the $\rho_{\text{In-BC}}$ can be calculated based on its mass concentration and

239 volume as follows:

$$\rho_{In-BC} = \frac{m_{In-BC}}{(\frac{\frac{m_{inorg}}{\rho_{inorg}}\kappa_{inorg} + \frac{m_{SOA}}{\rho_{SOA}}\kappa_{SOA}}{\kappa_{gf-MH}} - \frac{m_{inorg}}{\rho_{inorg}} - \frac{m_{SOA}}{\rho_{SOA}} - \frac{m_{In-POA}}{\rho_{POA}})} \qquad (9)$$

241 where, m_{In-BC} is the mass concentration of internally mixed BC, m_{inorg} and m_{SOA} are the

242 mass concentrations of the inorganic species and SOA, which are measured by the AMS.

243 m_{In-POA} is the mass concentrations of internally mixed POA and can be calculated

244 subtracting the mass fraction of NH-POA from the total mass concentrations of POA.

245 ρ_{inorg}, ρ_{SOA} and ρ_{POA} are the density of the inorganic species, SOA and POA. Since the

246 AMS measures the concentrations of the organic and inorganic ions, including SO_4^{2-},

247 NO_3^-, NH_4^+, Cl^-. Here inorganic species were derived by applying a simplified ion

248 pairing scheme (Gysel et al., 2007) to convert mass concentrations of ions to the

249 inorganic salts as follows:

251 $$n_{NH_4NO_3} = n_{NO_3^-}$$

252 $$n_{NH_4HSO_4} = \min(2n_{SO_4^{2-}} - n_{NH_4^+} + n_{NO_3^-}, n_{NH_4^+} - n_{NO_3^-})$$

253 $$n_{(NH_4)_2SO_4} = \max(n_{NH_4^+} - n_{NO_3^-} - n_{SO_4^{2-}}, 0)$$

250 $$n_{H_2SO_4} = \max(0, n_{SO_4^{2-}} - n_{NH_4^+} + n_{NO_3^-}) \qquad (10)$$

254 where n represents the number of moles, then the mass concentrations were obtained

255 by the number of moles times the molar mass of each inorganic salts. Because the

256 maximum value of the $n_{H_2SO_4}$ was zero in this campaign. Three inorganic salts

257 including NH_4HSO_4, $(NH_4)_2SO_4$, and NH_4NO_3 were applied in our study. The densities

258 for inorganic salts were taken from previous studies (Gysel et al., 2007; Wu et al., 2016).

259 Here the densities for three inorganics are 1.78, 1.77 and 1.72 g cm^{-3}, respectively. By

260 summarizing the previous studies (Gysel et al., 2007; Dinar et al., 2006), 1.4 g cm^{-3} was

261   selected as the density of SOA (ρ_{SOA}). The density of POA (ρ_{POA}) is assumed to be 1.0

262   g cm^{-3} for urban environments, which is similar to the lubricating oil (Wu et al., 2016).

263   Considering the cooking organic aerosols represent a high contribution to POA in urban

264   environments, a density of 0.85 g cm^{-3} chosen as the mean density for the rapeseed oil

265   and oleic acid (Reyes-Villegas et al., 2018) was also used to evaluated the result as

266   shown in section 2.3. The values of κ for inorganic components are 0.56 for NH_4HSO_4,

267   0.48 for $(NH_4)_2SO_4$ and 0.58 for NH_4NO_3, along with the best-fit values for the three

268   inorganic salts (Petters & Kreidenweis, 2007 and Gunthe et al., 2009). The κ_{SOA} is

269   assumed to be 0.15 according to the field studies in urban areas (Chang et al., 2010;

270   Kawana et al., 2016).

271   Note that, this method fails to retrieve the BC density when organics account for

272   a large fraction (>60 %). This is because that a higher fraction of OA usually

273   corresponds to lower total volume of all the species (Fig. S6), yielding negative values

274   for v_{In-BC} introduced in equation 11. As a result, 61 % of the data observed during the

275   campaign were valid for calculating the BC density.

276 $$v_{In-BC} = \frac{v_{inorg}\kappa_{inorg} + v_{SOA}\kappa_{SOA}}{\kappa_{gf-MH}} - v_{inorg} - v_{SOA} - v_{In-POA} \qquad (11)$$

277   Similarly, the bulk density of BC ($\rho_{bulk-BC}$) is calculated with the same method as

278   that for calculating the $\rho_{In-BC.}$ When calculating the $\rho_{bulk-BC}$, the bulk κ_{gf} value measured

279   by HTDMA is applied with the assumption of all the aerosol particles are internally

280   mixed.

2.3 Uncertainties and limitations

For the retrieval, the assumptions on the values of κ_{SOA}, ρ_{POA}, ρ_{SOA} and $\rho_{Ex\text{-}BC}$ as well as the fraction of primary organic aerosols in non-hygroscopic or hygroscopic mode would add uncertainty in the inferred values of ambient internally mixed BC density. For example, the freshly emitted POA particles might consistently be coated with the secondary particles during the aging process, resulting in changes of the $NF_{NH\text{-}POA}$. However, a real-time variation of the $NF_{NH\text{-}POA}$ is not yet available due to the lack of such measurements data. Applying the rough fractions of hydrophobic POA only under three different atmospheric conditions could still cause uncertainties. Also, the densities of POA and SOA may differ due to their precursors, emission sources and the formation mechanisms in ambient atmosphere (Alfarra et al., 2006; Reyes-Villegas et al., 2018). And the density of Ex-BC is generally characterized by the morphology and size (Wu et al., 2019). In addition, the value of κ_{SOA} spans largely due to the variability in the emissions of gas precursors and formation processes under different atmospheric conditions (Zhang et al., 2015; Liu et al., 2021b). Therefore, we examined the sensitivities of In-BC density to the variations of these factors, as exhibited in Fig. 1 and Fig.2.

The figures show that the In-BC density gradually decreases with the increment of the $NF_{NH\text{-}POA}$, implying the higher fraction of bare POA particles correspond to the early aging stage of aerosol particles. With increase of κ_{SOA}, the In-BC density is generally reduced, but with small fluctuations (Fig.1a, Fig. 2b). This suggests a complex impact of assumptions of κ_{SOA} on the retrieved BC density. In addition, the In-BC density

decreases very slightly as $\rho_{Ex\text{-}BC}$ increases (Fig. 2e), suggesting applying a larger $\rho_{Ex\text{-}BC}$ would derive smaller values for In-BC density. The In-BC density is insensitive to the changes of the density of POA and SOA, showing an almost negligible effect on the retrieved results (Fig. 2c and d).
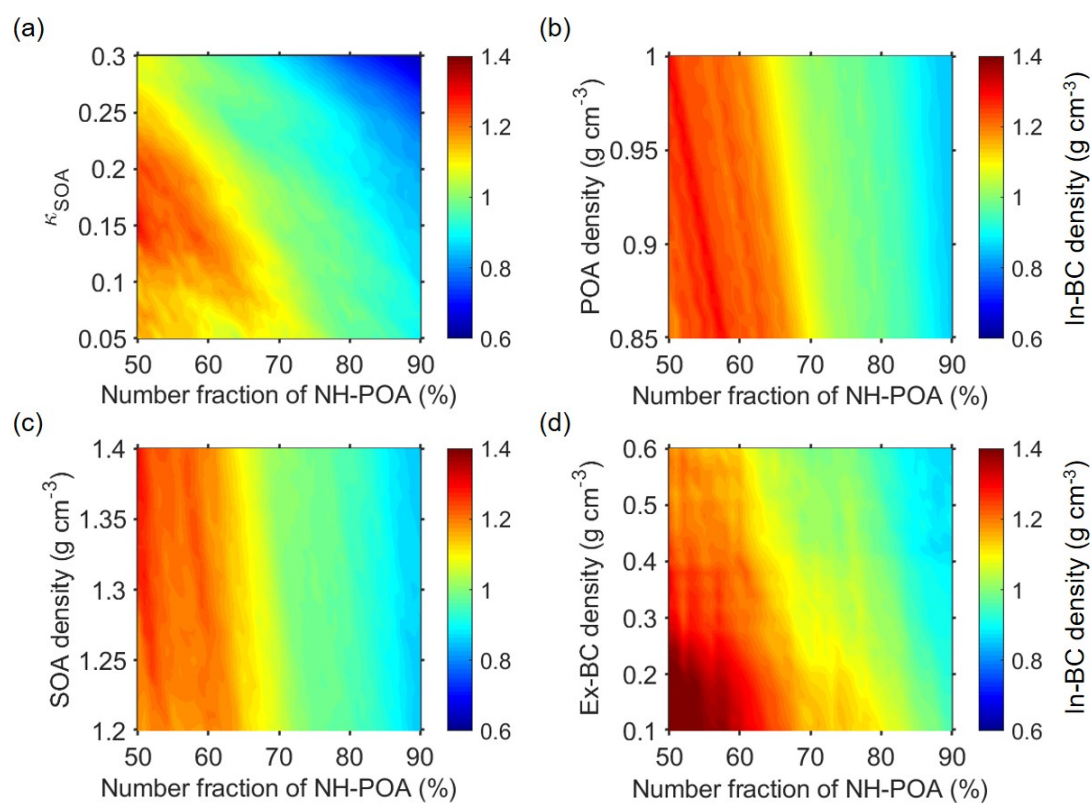
Figure 1. Sensitivities of In-BC density to the variations in the number fraction of nearly hydrophobic (NH) POA and hygroscopic parameter of OA (k_{SOA}) (a), POA density (b), SOA density (c) and the externally mixed BC density (d).
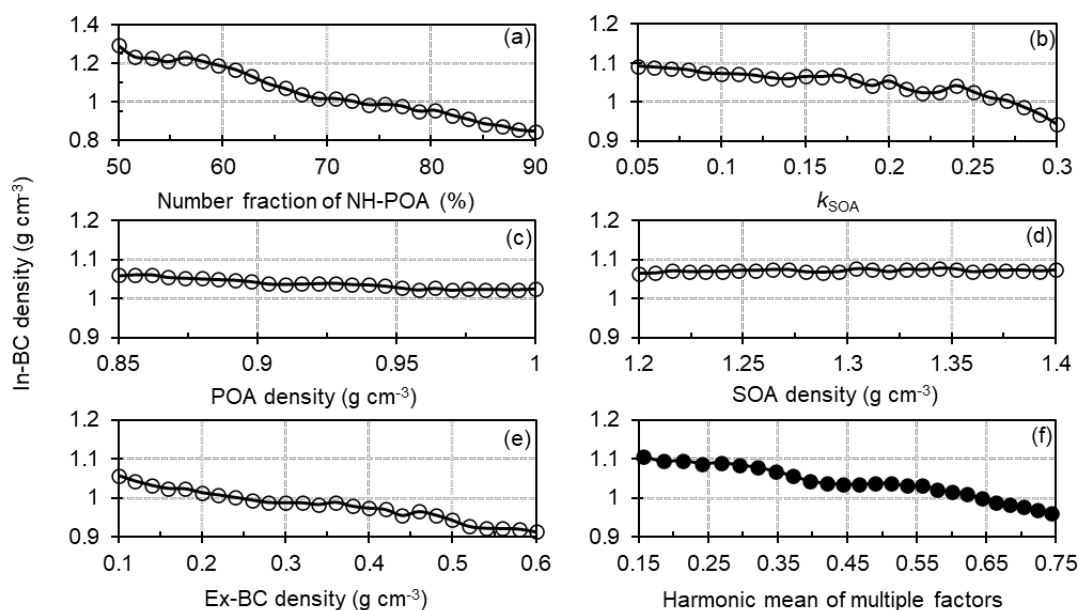
311

312 **Figure 2.** Sensitivity of the In-BC density to variations in the number fraction of nearly

313 hydrophobic (NH) POA (a), the hygroscopic parameter of SOA (b), the POA density

314 (c), the SOA density (d), the externally mixed BC density (e) and the harmonic mean

315 of multiple factors (f).

316   The uncertainty analysis shows that, by comparing the results based on the mean

317 fractions of the NF_{NH-POA} with a typical atmospheric observed range of 50-90 % for the

318 NF_{NH-POA} (Liu et al., 2021a), we show that the assumption on NF_{NH-POA} can lead to

319 relative deviations (uncertainty) of -17 %‒+27 % for the retrieved BC density (Fig.3a).

320   In addition, unlike inorganics (eg., NH_4HSO_4, $(NH_4)_2SO_4$ and NH_4NO_3), which

321 the hygroscopicity has been already well-understood (Petters and Kreidenweis, 2007),

322 the hygroscopicity of organic species varies largely due to the complexity in organic

323 aerosol constituents. Therefore, the assumption of the values of κ_{SOA} will add the

324 uncertainty in the calculation of BC density. Previous studies have suggested that the

325 organics has a wide range of κ values ranging from 0.05 to 0.3 (Jimenez et al., 2009;

326   Mei et al., 2013). Thus, the sensitivity test has also been done to examine the effect due

327   to changes in κ_{SOA} on calculating the density of BC (Fig. 1a). The result shows that the

328   assumption of κ_{SOA} value can cause an average relative deviation of -10 %–+3 % in

329   calculating the density of In-BC (Fig. 3b).
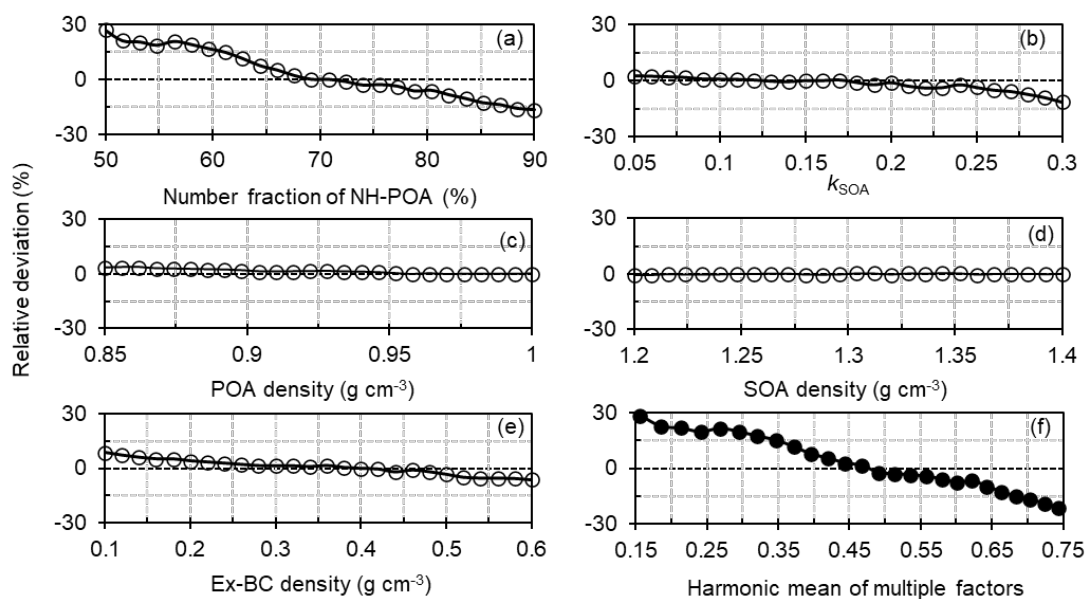
330

331   **Figure 3.** Relative deviations of the number fraction of nearly hydrophobic (NH) POA

332   to the In-BC density (a), the hygroscopic parameter of OA to the In-BC density (b), the

333   POA density to the In-BC density (c), the SOA density to the In-BC density (d), the

334   externally-mixed BC density to In-BC density (e) and the combined deviations based

335   on multiple factors mentioned above (f).

336   However, the sensitivity test shows that the impact of both the ρ_{POA} and ρ_{SOA}

337   variations on the BC density estimation is very small or even negligible (Fig. 1b, c). By

338   varying the ρ_{POA} from 0.85 to 1.0 g cm^{-3} and the ρ_{SOA} from 1.2 to 1.4 g cm^{-3} according

339   to the literatures (Noureddini et al., 1992; Alfarra et al., 2006; Reyes-Villegas et al.,

340   2018), the retrieval uncertainties in the BC density are within ±5 % and ±1 %

341   respectively (Fig. 3c, d). For ρ_{Ex-BC}, it exhibits that the evolution of the ρ_{Ex-BC} could lead

342 to an average deviation of ± 10 % in calculating In-BC density (Fig. 3e) when

343 increasing the values of $\rho_{\text{Ex-BC}}$ from 0.1 to 0.6 g cm^{-3}, which represents a typical range

344 in ambient atmosphere (Wu et al., 2019; Liu et al., 2020). A combined uncertainty (δ)

345 caused by the multiple factors (δ_i), which is calculated by equation 12, is -21 %−+29 %

346 as shown in Fig. 3f.

347
$$\delta = \sqrt{\sum_{i=1}^{n} \delta_i{}^2} \tag{12}$$

348 **3 Results and Discussion**

349 **3.1 Retrieved mixing state and density of BC: comparison and validation**

350 Figure 4a shows retrieved time series of the mixing state of ambient BC during the

351 campaign. Large temporal variations of the mass fraction of internally and externally

352 mixed BC are presented during the observed period at the sites. The temporal changes

353 should be related to the atmospheric aging process or diurnal variations of emissions

354 (Liu et al., 2019a; Fan et al., 2020). Statistically, the average mass fraction of externally

355 and internally mixed BC is 20±18 % and 80±20 % respectively, showing that most of

356 the BC particles were aged and internally mixed with other components. Previous

357 studies at urban sites have shown that the co-existence of the externally mixed BC in

358 the ambient atmosphere (Schwarz et al., 2008; Cheng et al., 2012; Chen et al., 2020)

359 due to continuous combustion processes (e.g., vehicle exhaust and residential sector)

360 (Wang et al., 2017; Liu et al., 2019a). Our results are basically comparable with those
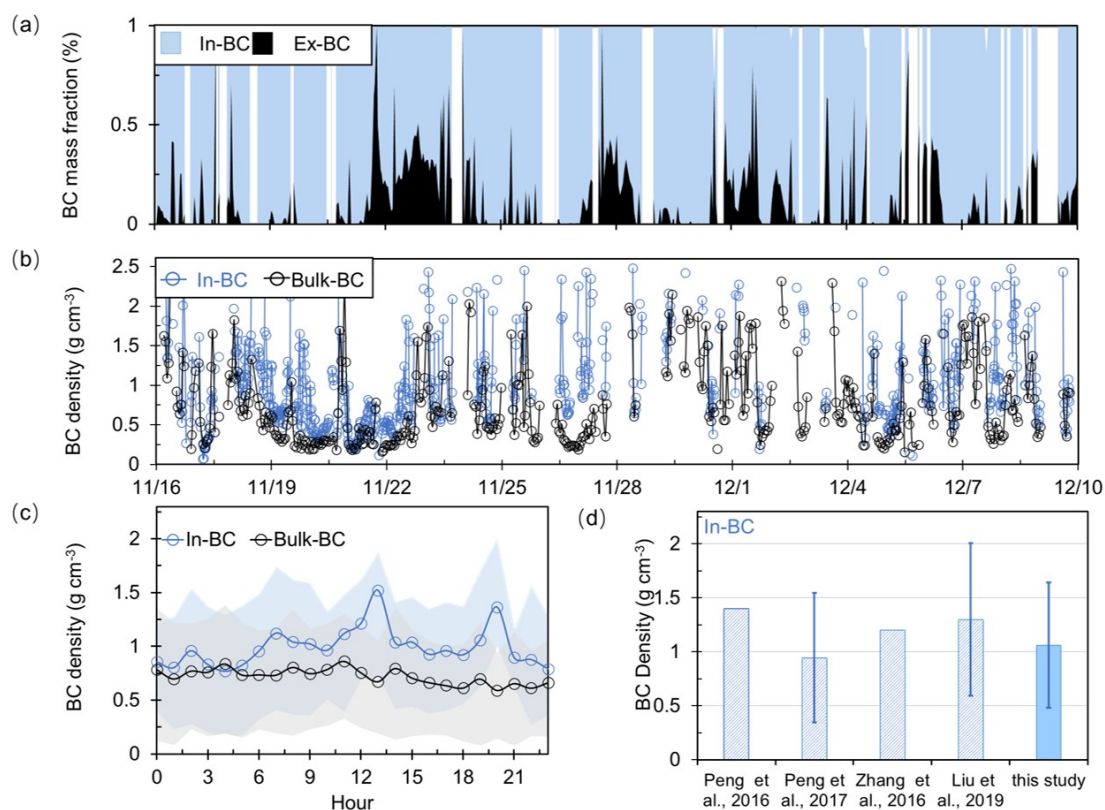
Figure 4. (a) Time series of the mass fraction of the retrieved internal- and external-mixed BC; (b) Time series of the retrieved density of the bulk and internal- mixed BC (In-BC); (c) Diurnal variation of the retrieved density of bulk and In-BC; (d) Comparison of the results of the derived In-BC density in this study with that reported in literatures.

directly measured or indirectly retrieved previously reported results. For example, Chen et al., 2020 found that the mass fraction of internally mixed BC particles was nearly to be ~80−90 % in summer of Beijing based on VTDMA measurements. Liu et al. (2020), using a tandem system with an aerodynamic aerosol classifier and SP2, reported that the mass fraction of internally BC-containing particles would increase with increasing size and reach ~70 % in Beijing. Overall, the mass fraction obtained in our study is comparable with those reported in urban Beijing. Previous studies also displayed that

374 the significant diversity of the BC mixing state among emission conditions and coating

375 process (Shiraiwa et al., 2008; Pan et al., 2017; Zhang et al., 2020b). Accordingly, the

376 densities of the bulk and internally mixed BC present apparent fluctuations as shown in

377 Fig. 4b, which is significantly affected by the variations of BC emission sources and its

378 rapid aging process. The density of the In-BC during daytime was generally higher than

379 that at night (Fig. 4c). The elevated BC density during daytime is likely due to that the

380 strong photochemical processes promote the aging of BC particles, which resulted in a

381 conversion from uncompacted structure to compact and regular spherical shapes of BC

382 (Qiao et al., 2018; Liu et al., 2019b; Zhou et al., 2022). The lift in BC density around

383 20:00 LT might indicate that the BC particles would be rapidly coated with the SIA

384 particles and continuously aged in the polluted period due to the heterogeneous

385 reactions of SIA in urban regions (Zhang et al., 2016; Peng et al., 2017). Actually,

386 following the haze evolution, the fraction of nearly hydrophobic group reduced rapidly

387 (Fig. S7). Consequently, the average density of In-BC increased obviously from the

388 clean conditions to the polluted periods (Fig. S8). A slight decrease was observed in the

389 bulk BC density during traffic hours. This is likely associated with the continues

390 emissions (e.g., vehicle exhaust) that lead to uncoated or uncompacted BC particles in

391 this period. The diurnal cycle in In-BC density is consistent with the coating thickness

392 measured by a tandem CPMA-SP2-DMA-SP2 (Liu et al., 2020), demonstrating that the

393 new method can derive the density of ambient BC particles reasonably. Averagely, the

394 bulk and internally mixed BC densities are with campaign averaged values of 0.7±0.5

395 and 1.1±0.6 g cm^{-3} respectively, which are much less than 1.8 g cm^{-3}, implying that the

396 BC particles is not a void-free spheres in the urban atmosphere. The results of In-BC

397 density are comparable with that observed at the other sites in North China Plain (NCP)

398 as shown in Fig. 4d, illustrating that the BC effective density retrieved by this method

399 is within the range of field measurements.
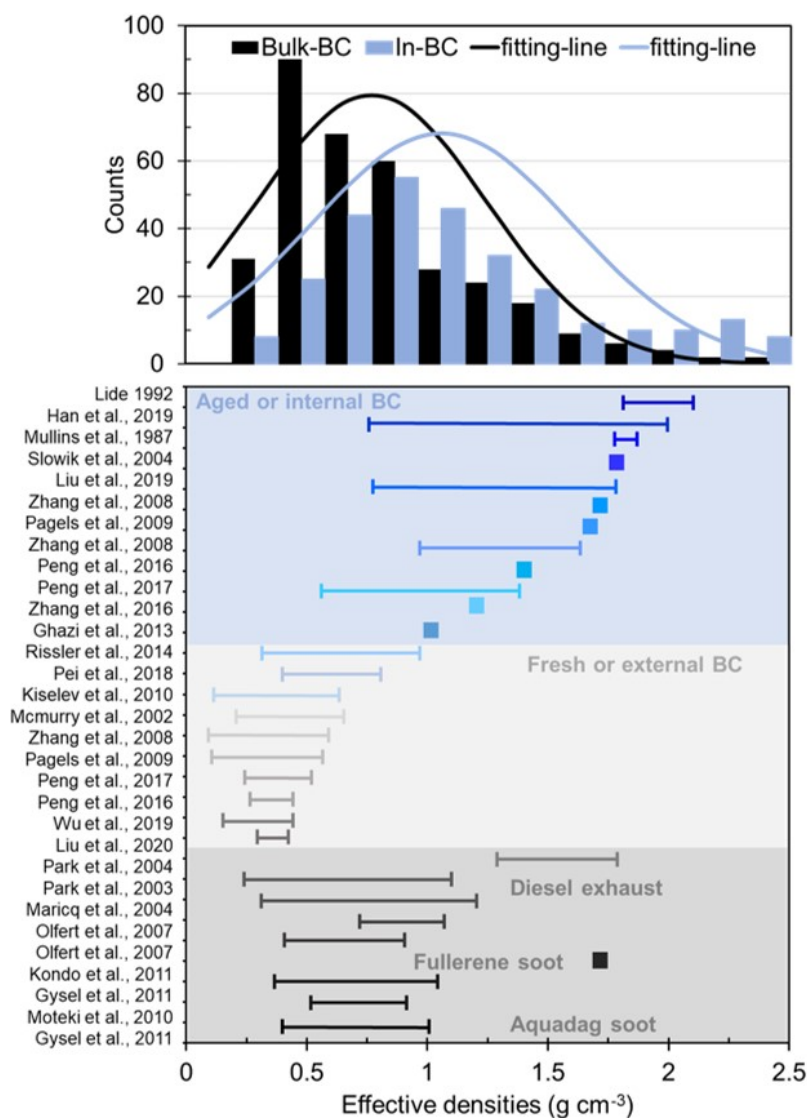
400

401 **Figure 5.** The probability distribution function (PDF) of the retrieved density of bulk

402 and In-BC and the measured density distribution spectrum of BC from different sources

403 reported in literatures.

404   Based on both field measurements (e.g. Lide 1992; Zhang et al., 2016; Wu et al.,

405 2019; Liu et al., 2019b) and laboratory studies (e.g. McMurry et al., 2002; Park et al.,

406   2003, 2004; Olfert et al., 2007; Kiselev et al., 2010; Gysel et al., 2011, 2012), the BC

407   density from diverse combustion sources or representing different aging degree has

408   been obtained and ranges widely from 0.14 to 2.1 g cm^{-3}, as has been summarized and

409   shown in Fig. 5. Mean probability distribution function (PDF) of the density of bulk

410   and In-BC retrieved by this study is also presented in Fig. 5. It shows that the retrieved

411   density of bulk BC exhibits a dominant mode with a peak value of 0.7 g cm^{-3}, which is

412   situated between the typical density range of those externally mixed and internally

413   mixed BC measured previously. For the In-BC, the PDF is with a peak value at 1.1 g

414   cm^{-3}, but ranges widely from ~0.5 to 2.5 g cm^{-3}, which indicates various morphologies,

415   different aging degree and compositions of ambient BC particles due to the complex

416   impact of multiple local sources and aging processes during the observed period in

417   urban Beijing. Overall, the retrieved values for In-BC fall within the range of typical

418   internal mixed BC reported in the literatures, verifying the reliability of our inversion

419   results.

420   **3.2 Sensitivity of predicted N_{CCN} to changes of BC density**

421   A previous study showed that the use of an inaccurate density value of BC particles

422   would result in large bias in estimating κ of ambient aerosol particles with the ZSR

423   mixing rule (Fan et al., 2020), as would further lead to uncertainties in prediction of

424   N_{CCN} and relevant climate effects. Considering the large variation range of BC density

425   during the campaign, which is closely associated with its morphology or degree of its

426   aging, we further examine the sensitivity of critical supersaturation (S_c), critical

427   diameter (D_{cut}) and predicted N_{CCN} to variations of BC density (Fig. 6). Here, we use

428   the critical diameter and particle number size distribution to calculate N_{CCN}. The method

429   to derive the critical diameter is based on Köhler theory and ZSR rule.
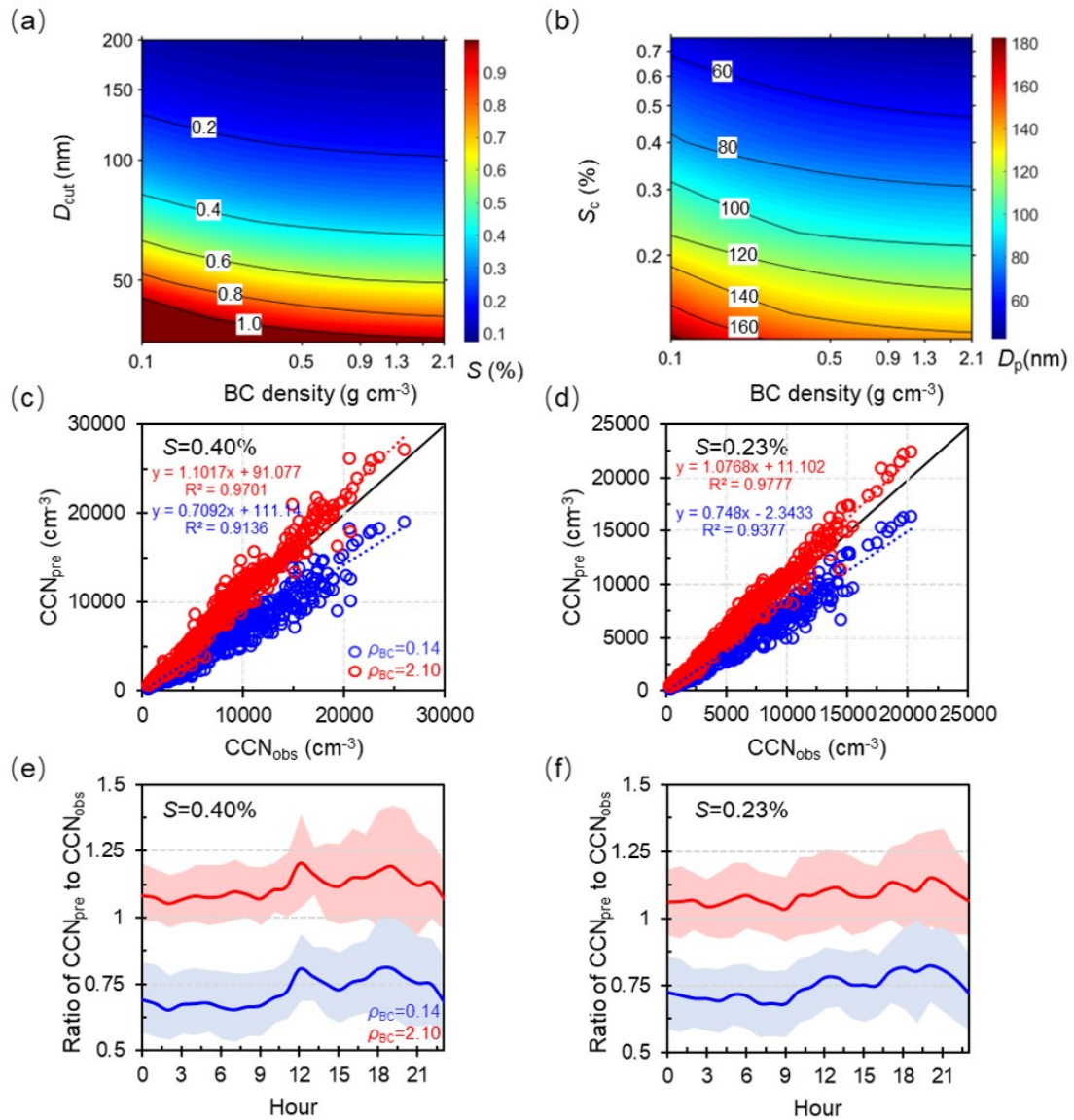
430

431   **Figure 6.** Sensitivity of critical supersaturation (S_c) (a) and diameter (D_{cut}) (b) to the

432   variations in BC density; Predicted N_{CCN} as a function of measured N_{CCN} by varying the

433   density from 0.14 to 2.1 g cm^{-3} at S=0.40 % (c) and S=0.23 % (d), the black solid line

434   is the 1:1 line; Diurnal variations in the ratio of predicted-to-measured N_{CCN} at S=0.40 %

435   (e) and S=0.23 % (f).

436   The results show that, by varying the value of density from 0.14 to 2.1 g cm^{-3} that

437   represents the lower and upper limit of BC density in the atmosphere, the D_{cut} reduces

438   apparently at a given supersaturation (S) (Fig. 6a), or similarly, the S_c decreases rapidly

439   for a given particle size (Fig. 6b). The results show that the changes of the D_{cut} and S_c

440   are more sensitive when the BC density is below 1.0 g cm^{-3}. And the effects on the D_{cut}

441   and S_c both gradually weakened with the increase of BC density. This shows that it is

442   critical to apply more accurate BC density for the aerosol particles with low aging

443   degree in predicting CCN and its climate effect. Accordingly, the ratios of predicted-

444   to-measured N_{CCN} ranged from 0.72 to 1.11 by varying the BC density from 0.14 to 2.1

445   g cm^{-3} at the typical S of 0.23 % and 0.40 % (Fig. 6c, 6d), showing an estimation

446   uncertainty of -28 %–11 % in N_{CCN} prediction.

447   The diurnal variations in the ratio of predicted-to-measured N_{CCN} at S=0.40 % and

448   0.23 % are shown to examine the response of the BC density on N_{CCN} prediction at

449   different time periods (Fig. 6e, 6f). By applying the lower limit of density value of 0.14

450   g cm^{-3}, the prediction is much worse compared to the use of the density of 2.1 g cm^{-3} at

451   nighttime (00:00-06:00 LT), when the latter is much closer to the real density of ambient

452   BC (Fig. 4c). The prediction is improved substantially by applying the value of 0.14 g

453   cm^{-3} during evening rush hours (18:00-20:00 LT), during which the ambient BC

454   particles is disturbed by the traffic emissions (Fig. 4c). And now, the prediction becomes

455   worse by applying the value of 2.1 g cm^{-3}, and an obvious overestimation by up to ~40 %

456   is shown. The results further illustrate that it is critical to account for the real-time

457   mixing state and density of BC particles in N_{CCN} prediction, particularly in those regions

458 with heavy traffic and residential coal emissions.

459 It should be noted that the assumption of the surface tension of water would

460 overestimate the critical diameter and underpredict CCN number concentration. While

461 the surface tension depression might be more obvious for the small size particles (<60

462 nm), as the fraction of organics are higher at small particles size (Meng et al., 2014; Cai

463 et al., 2018). Here, in this study, we calculated the critical diameters at supersaturations

464 of 0.40 % and 0.23 %, typical values in cloud, corresponding to larger sizes (> 70 nm

465 and 90 nm) of aerosols. Therefore, the uncertainties from the application of the surface

466 tension of pure water should be negligible (< 10 %). Here, three schemes were assumed

467 to evaluate the effect of BC density and mixing state on prediction of CCN number

468 concentrations. The detailed calculation methods are presented in the supporting

469 information (SI: Methods) or referenced from Ren et al., 2018.

470 **3.3 Using the real-time variations of BC density and mixing state to predict N_{CCN}**

471 Figure 7 exhibits the comparisons between predicted and measured N_{CCN} at S of

472 0.23 % and 0.40 % by accounting for the retrieved real-time variations of BC density

473 and mixing state. It shows that the N_{CCN} can be well predicted with a slope of 1.01 and

474 1.02 at S of 0.23 % and 0.40 % respectively (Fig. 7a, 7b), only presenting a slight

475 deviation. The slight deviation is primarily due to the fixed value of the density for the

476 externally mixed BC caused by the retrieved method, especially during noontime and

477 evening rush periods (Fig. 7c and 7d).
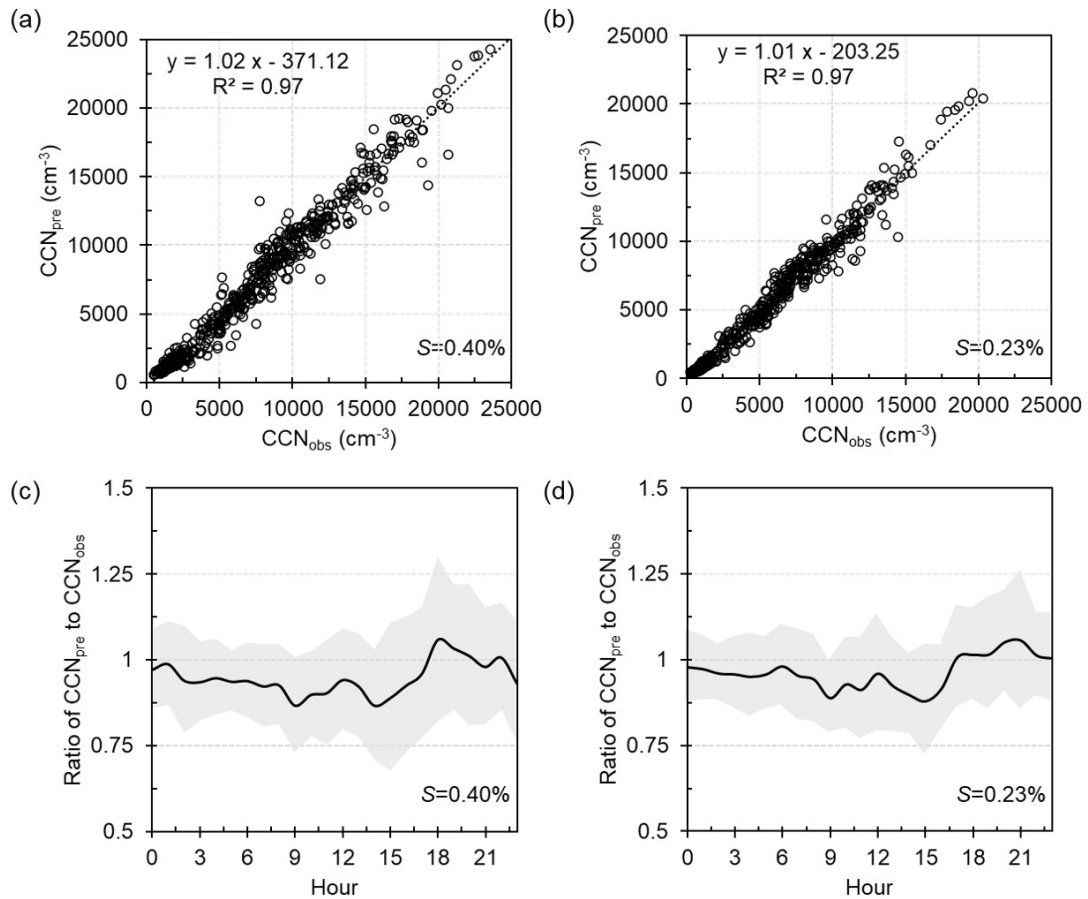
Figure 7. Prediction CCN number concentration using the mixing state and In-BC density derived from HTDMAs at S=0.40 % (a) and S=0.23 % (b). Diurnal variations in the ratio of predicted-to-measured N_{CCN} at S=0.40 % (c) and S=0.23 % (d).

The diurnal variations in the ratio of predicted-to-measured N_{CCN} shows the N_{CCN} can be underestimated by up to 15 % at S=0.40 % during those periods. While, a slightly overrated during the evening traffic hours and nighttime may be due to the underestimation of the number fraction of Ex-BC. Overall, the dependence of the CCN prediction on S is due to the size dependence of κ and mixing state (Zhang et al., 2017; Liu et al., 2020; Xu et al., 2021). The better closure at S=0.23 % is because that the bulk κ of particles is closer to that the critical diameter corresponding to S=0.23 %, with D_p of 100-150 nm. Similarly, the effect on CCN prediction induced by the bulk mixing

490   state would be more critical for smaller particles, corresponding to the critical diameter

491   at high S.

492   Overall, when considering the effective density of BC relevant to its mixing state,

493   the CCN closure achieves. Previous studies have shown that the fresh emitted BC

494   particles may convert from fractal-like aggregates to a compact structure and its density

495   would increase with the aging process (Pagels et al., 2009; Rissler et al., 2014; Peng et

496   al., 2016; Liu et al., 2019b; Zhang et al., 2020a, 2022), but the actual density of In-BC

497   may be lower than 1.8 g cm^{-3} in the ambient atmosphere according to this study.

498   Therefore, the currently applied value represents a density of the void-free structure of

499   BC particles may cause an overestimation in CCN prediction.

500   **4 Conclusions**

501   The mixing state and effective density of BC changed through heterogenous

502   chemistry process and thus would cause uncertainty in evaluating its CCN activity. In

503   this study, we develop a new method to retrieve the mixing state and effective density

504   of ambient BC using field measurements and the Köhler theory. The uncertainty of the

505   new retrieval method was evaluated within ±30 %, which is primarily caused to

506   assuming the κ_{SOA} and the fraction of primary organic aerosols in non-hygroscopic or

507   hygroscopic mode. The retrieved results show that most of the BC particles were aged

508   and internally mixed with other components, with mean mass fraction of 80±20 %.

509   Averagely, the retrieved densities of the bulk and internal-mixed BC are 0.7±0.5 and

510   1.1±0.6 g cm^{-3} respectively, but ranges widely from ~0.1 to 2.5 g cm^{-3}, indicating

various morphologies, different aging degree and compositions of ambient BC particles due to the complex impact of multiple local sources and aging processes during the observed period. The retrieved results are basically comparable with the previous observations in North China Plain.

Further examination shows the N_{CCN} prediction is with uncertainties of -28 %−11 % at the typical S of 0.23 % and 0.40 % by varying the BC density from 0.14 to 2.1 g cm^{-3} that represents the lower and upper limit of ambient BC particles. Moreover, the prediction is found more sensitive to the variability of BC density when it is <1.0 g cm^{-3}, suggesting a great significance to account for the effect of BC density for the aerosol particles with low aging degree when evaluating the climate effect. The CCN closure achieves when introducing the retrieved real-time BC density relevant to its mixing state. This work provides a unique way of utilizing field observations to infer ambient BC density and highlights the current assumption of a void-free structure of BC particles in models would cause large uncertainties in CCN prediction and in the relevant climate effect evaluation.

Data availability.

All data needed to evaluate the conclusions in the paper are present in the paper and/or the Supplement. All data used in the study are also available from the corresponding author upon request (zhangfang2021@hit.edu.cn).

Author contributions.

FZ and JR conceived the conceptual development of the manuscript. JR directed and performed of the experiments with JL, LC, and FZ. JR conducted the data analysis and wrote the draft of the manuscript. All authors edited and commented on the various sections of the manuscript.

Acknowledgments.

This work was funded by the National Natural Science Foundation of China (NSFC) research project (41975174, 41675141). We thank all participants in the field campaigns for their tireless work and cooperation. We also thank Dr. Yele Sun and his group for providing the data of nonrefractory submicron aerosol chemical composition.

Competing interests.

The contact author has declared that neither they nor their co-authors have any competing interests.

References

Alfarra, M. R., Paulsen, D., Gysel, M., Garforth, A. A., Dommen, J., Prévôt, A. S. H., Worsnop, D. R., Baltensperger, U., and Coe, H.: A mass spectrometric study of secondary organic aerosols formed from the photooxidation of anthropogenic and biogenic precursors in a reaction chamber, Atmos. Chem. Phys., 6, 5279– 5293, https://doi:10.5194/acp-6-5279-2006, 2006.

Bond, T. C., Doherty, S. J., Fahey, D., Forster, P., Berntsen, T., DeAngelo, B., Flanner, M., Ghan, S., Kärcher, B., and Koch, D.: Bounding the role of black carbon in the

climate system: A scientific assessment, J. Geophys. Res.-Atmos., 118(11), 5380–5552, https://doi.org/10.1002/jgrd.50171, 2013

Clarke, A.D., Shinozuka, Y., Kapustin, V.N., Howell, S., Huebert, B., Doherty, S., Anderson, T., Covert, D., Anderson, J., Hua, X., Moore II, K.G., McNaughton, C., Carmichael, G., Weber, R.: Size distributions and mixtures of dust and black carbon aerosol in Asian outflow: physiochemistry and optical properties, J. Geophys. Res.-Atmos., 109, D15S09, https://doi.org/10.1029/2003JD004378, 2004.

Cheng, Y. F., Su, H., Rose, D., Gunthe, S. S., Berghof, M., Wehner, B., Achtert, P., Nowak, A., Takegawa, N., Kondo, Y., Shiraiwa, M., Gong, Y. G., Shao, M., Hu, M., Zhu, T., Zhang, Y. H., Carmichael, G. R., Wiedensohler, A., Andreae, M. O., and Pöschl, U.: Size-resolved measurement of the mixing state of soot in the megacity Beijing, China: diurnal cycle, aging and parameterization, Atmos. Chem. Phys., 12, 4477–4491, https://doi.org/10.5194/acp-12-4477-2012, 2012.

Cheng, Y. F., Eichler, H., Wiedensohler, A., Heintzenberg, J., Zhang, Y. H., Hu, M., Herrmann, H., Zeng, L. M., Liu, S., Gnauk, T., Brüggemann, E., and He, L. Y.: Mixing state of elemental carbon and non-light-absorbing aerosol components derived from in situ particle optical properties at Xinken in Pearl River Delta of China, J. Geophys. Res., 111, D20204, doi:10.1029/2005JD006929, 2006.

Chen, L., F. Zhang, P. Yan, X. Wang, L. Sun, Y. Li, X. Zhang, Y. Sun, and Z. Li.: The large proportion of black carbon (BC)-containing aerosols in the urban atmosphere, Environ. Pollut., 263, 114507, https://doi.org/10.1016/j.envpol.2020.114507, 2020.

Chang, R. Y.-W., Slowik, J. G., Shantz, N. C., Vlasenko, A., Liggio, J., Sjostedt, S. J., Leaitch, W. R., and Abbatt, J. P. D.: The hygroscopicity parameter (k) of ambient organic aerosol at a field site subject to biogenic and anthropogenic influences: relationship to degree of aerosol oxidation, Atmos. Chem. Phys., 10, 5047–5064, https://doi:10.5194/acp-10-5047-2010, 2010.

Cai, M., Tan, H., Chan, C. K., Qin, Y., Xu, H., Li, F., Schurman, M. I., Liu, L., and Zhao, J.: The size-resolved cloud condensation nuclei (CCN) activity and its prediction based on aerosol hygroscopicity and composition in the Pearl Delta River (PRD) region during wintertime 2014, Atmos. Chem. Phys., 18, 16419–16437, https://doi.org/10.5194/acp-18-16419-2018, 2018.

Dinar, E., Mentel, T. F., and Rudich, Y.: The density of humic acids and humic like substances (HULIS) from fresh and aged wood burning and pollution aerosol particles, Atmos. Chem. Phys., 6, 5213–5224, doi:10.5194/acp-6-5213-2006, 2006.

Dameto de España, C., Wonaschütz, A., Steiner, G., Rosati, B., Demattio, A., Schuh, H., and Hitzenberger, R.: Long-term quantitative field study of New Particle Formation (NPF) events as a source of Cloud Condensation Nuclei (CCN) in the urban background of Vienna, Atmos. Environ., 164, 289–298, https://doi.org/10.1016/j.atmosenv.2017.06.001, 2017.

Flanner, M. G., Zender, C. S., Randerson, J. T., and Rasch, P. J.: Present-day climate forcing and response from black carbon in snow, J. Geophys. Res.-Atmos., 112, D11202, https://doi.org/10.1029/2006JD008003, 2007.

Fan, X., Liu, J., Zhang, F., Chen, L., Conllins, D., Xu, W., Jin, X., Ren, J., Wang, Y.,Wu, H., Li, S., Sun, Y., Li, Z.: Contrasting size-resolved hygroscopicity of fine particles

derived by HTDMA and HR-ToF-AMS measurements between summer and winter in Beijing: the impacts of aerosol aging and local emissions, Atmos. Chem. Phys. 20, 915-929, https://doi.org/10.5194/acp-20-915-2020, 2020.

Geller, M., Biswas, S., and Sioutas, C.: Determination of particle effective density in urban environments with a differential mobility analyzer and aerosol particle mass analyzer, Aerosol Sci. Technol., 40, 709–723, https://doi.org/10.1080/02786820600803925, 2006.

Gysel, M., McFiggans, G. B., and Coe, H.: Inversion of tandem differential mobility analyser (TDMA) measurements, J. Aerosol Sci., 40, 134–151, https://doi.org/10.1016/j.jaerosci.2008.07.013, 2009.

Gysel, M., Crosier, J., Topping, D. O., Whitehead, J. D., Bower, K. N., Cubison, M. J., Williams, P. I., Flynn, M. J., McFiggans, G. B., and Coe, H.: Closure study between chemical composition and hygroscopic growth of aerosol particles during TORCH2, Atmos. Chem. Phys., 7, 6131–6144, https://doi.org/10.5194/acp-7-6131-2007, 2007.

Gunthe, S. S., King, S. M., Rose, D., Chen, Q., Roldin, P., Farmer, D. K., Jimenez, J. L., Artaxo, P., Andreae, M. O., Martin, S. T., and Pöschl, U.: Cloud condensation nuclei in pristine tropical rainforest air of Amazonia: size resolved measurements and modeling of atmospheric aerosol composition and CCN activity, Atmos. Chem. Phys., 9, 7551–7575, https://doi.org/10.5194/acp-9-7551-2009, 2009.

Gysel, M., Laborde, M., Olfert, J. S., Subramanian, R., & Gröhn, A. J.: Effective density of aquadag and fullerene soot black carbon reference materials used for SP2 calibration, Atmos. Meas. Tech., 4(12), 4937–4955, https://doi.org/10.5194/amt-4-2851-2011, 2011.

Gysel, M., Laborde, M., Mensah, A. A., Corbin, J. C., Keller, A., Kim, J., et al.: Technical note: The single particle soot photometer fails to reliably detect PALAS soot nanoparticles, Atmos. Meas. Tech., 5(12), 3099–3107, https://doi.org/10.5194/amt-5-3099-2012, 2012.

Jimenez, J. L., Canagaratna, M. R., Donahue, N. M., Prevot, A. S. H., Zhang, Q., Kroll, J. H., DeCarlo, P. F., Allan, J. D., Coe, H., Ng, N. L., Aiken, A. C., Docherty, K. S., Ulbrich, I. M., Grieshop, A. P., Robinson, A. L., Duplissy, J., Smith, J. D., Wilson, K. R., Lanz, V. A., Hueglin, C., Sun, Y. L., Tian, J., Laaksonen, A., Raatikainen, T., Rautiainen, J., Vaattovaara, P., Ehn, M., Kulmala, M., Tomlinson, J. M., Collins, D. R., Cubison, M. J., Dunlea, E. J., Huffman, J. A., Onasch, T. B., Alfarra, M. R., Williams, P. I., Bower, K., Kondo, Y., Schneider, J., Drewnick, F., Borrmann, S., Weimer, S., Demerjian, K., Salcedo, D., Cottrell, L., Griffin, R., Takami, A., Miyoshi, T., Hatakeyama, S., Shimono, A., Sun, J. Y., Zhang, Y. M., Dzepina, K., Kimmel, J. R., Sueper, D., Jayne, J. T., Herndon, S. C., Trimborn, A. M., Williams, L. R., Wood, E. C., Middlebrook, A. M., Kolb, C. E., Baltensperger, U., and Worsnop, D. R.: Evolution of Organic Aerosols in the Atmosphere, Science., 326, 1525–1529, https://doi.org/10.1126/science.1180353, 2009.

Kiselev, A., Wennrich, C., Stratmann, F., Wex, H., Henning, S., Mentel, T.F., Kiendler-Scharr, A., Schneider, J., Walter, S., Lieberwirth, I.: Morphological characterization of soot aerosol particles during LACIS Experiment in November (LExNo), J. Geophys. Res. -Atmos., 115, D11204. https://doi.org/10.1029/2009jd012635, 2010.

639 Khalizov, A. F., Zhang, R., Zhang, D., Xue, H., Pagels, J., and McMurry, P. H.:
640   Formation of highly hygroscopic soot aerosols upon internal mixing with sulfuric
641   acid   vapor,   J.   Geophys.   Res.-Atmos.,   114,   D05208,
642   https://doi.org/10.1029/2008jd010595, 2009.
643 Kawana, K., Nakayama, T., and Mochida, M.: Hygroscopicity and CCN activity of
644   atmospheric aerosol particles and their relation to organics: Characteristics of urban
645   aerosols in Nagoya, Japan, J. Geophys. Res.-Atmos., 121, 4100–4121,
646   https://doi.org/10.1002/2015JD023213, 2016.
647 Li, M., Zhang, Q., Kurokawa, J.-I., Woo, J.-H., He, K., Lu, Z., Ohara, T., Song, Y.,
648   Streets, D. G., Carmichael, G. R., Cheng, Y., Hong, C., Huo, H., Jiang, X., Kang, S.,
649   Liu, F., Su, H., and Zheng, B.: MIX: a mosaic Asian anthropogenic emission
650   inventory under the international collaboration framework of the MICS-Asia and
651   HTAP, Atmos. Chem. Phys., 17, 935–963, https://doi.org/10.5194/acp-17-935-2017,
652   2017.
653 Liu, D., Joshi, R., Wang, J., Yu, C., Allan, J. D., Coe, H., Flynn, M. J., Xie, C., Lee, J.,
654   Squires, F., Kotthaus, S., Grimmond, S., Ge, X., Sun, Y., and Fu, P.: Contrasting
655   physical properties of black carbon in urban Beijing between winter and summer,
656   Atmos. Chem. Phys., 19, 6749–6769, https://doi.org/10.5194/acp-19-6749-2019,
657   2019a.
658 Liu, D., Allan, J., Whitehead, J., Young, D., Flynn, M., Coe, H., McFiggans, G.,
659   Fleming, Z. L., and Bandy, B.: Ambient black carbon particle hygroscopic properties
660   controlled by mixing state and composition, Atmos. Chem. Phys., *13*, 2015–2029,
661   https://doi.org/10.5194/acp-13-2015-2013, 2013.
662 Liu, H., Pan, X.L., Wu, Y., Wang, D.W., Tian, Y., Liu, X.Y., et al.: Effective densities of
663   soot particles and their relationships with the mixing state at an urban site in the
664   Beijing megacity in the winter of 2018, Atmos. Chem. Phys. 19, 14791–14804,
665   https://doi.org/10.5194/acp-19-14791-2019, 2019b.
666 Lide, D. R. (ed.). CRC Handbook of Chemistry and Physics. CRC Press: Ann Arbor,
667   MI. (1992).
668 Lance, S., Medina, J., Smith, J., and Nenes, A.: Mapping the operation of the DMT
669   continuous   flow   CCN   counter,   Aerosol   Sci.   Tech.,   40,   242–254,
670   https://doi.org/10.1080/02786820500543290, 2006.
671 Liu, H., Pan, X., Liu, D., Liu, X., Chen, X., Tian, Y., Sun, Y., Fu, P., and Wang, Z.:
672   Mixing characteristics of refractory black carbon aerosols at an urban site in Beijing,
673   Atmos. Chem. Phys., 20, 5771–5785, https://doi.org/10.5194/acp-20-5771-2020,
674   2020.
675 Liu, L, Zhang, J, Zhang, Y, Wang, Y, Xu, L, Yuan, Q, et al.: Persistent residential
676   burning-related primary organic particles during wintertime hazes in North China:
677   insights into their aging and optical changes, Atmos. Chem. Phys. *21,* 2251–2265,
678   https://doi.org/10.5194/acp-21-2251-2021, 2021a.
679 Liu, J., Zhang, F., Xu, W., Sun, Y., Chen, L., Li, S.: Hygroscopicity of organic aerosols
680   linked to formation mechanisms, Geophysical Research Letters, 48, e2020GL091683,
681   https://doi.org/10.1029/2020gl091683, 2021b.
682 McMurry, H. Peter, Wang Xin, Park Kihong & Ehara Kensei.: The Relationship

between Mass and Mobility for Atmospheric Particles: A New Technique for Measuring Particle Density, Aerosol Sci. Technol., 36:2, 227-238, https://doi.10.1080/027868202753504083, 2002.

Massoli, P., Onasch, T.B., Cappa, C.D., Nuamaan, I., Hakala, J., Hayden, K., Li, S.M., Sueper, D.T., Bates, T.S., Quinn, P.K., Jayne, J.T., Worsnop, D.R.: Characterization of black carbon-containing particles from soot particle aerosol mass spectrometer measurements on the R/V Atlantis during CalNex 2010, J. Geophys. Res.- Atmos., 120, 2575-2593, https://doi.org/10.1002/2014JD022834, 2015.

Mei, F., Setyan, A., Zhang, Q., and Wang, J.: CCN activity of organic aerosols observed downwind of urban emissions during CARES, Atmos. Chem. Phys., 13, 12155–12169, https://doi.org/10.5194/acp-13-12155-2013, 2013.

Meng, J. W., Yeung, M. C., Li, Y. J., Lee, B. Y. L., and Chan, C. K.: Size-resolved cloud condensation nuclei (CCN) activity and closure analysis at the HKUST Supersite in Hong Kong, Atmos. Chem. Phys., 14, 10267–10282, https://doi.org/10.5194/acp-14-10267-2014, 2014.

Noureddini, H., Teoh, B. C., Davis Clements, L.: Densities of vegetable oils and fatty acids, J. Am. Oil Chem. Soc., 69 (12), 1184−1188, 1992.

Olfert, J. S., Symonds, J. P. R., and Collings, N.: The effective density and fractal dimension of particles emitted from a light-duty diesel vehicle with a diesel oxidation catalyst, J. Aerosol Sci., 38, 69–82, https://doi.org/10.1016/j.jaerosci.2006.10.002, 2007.

Park, K., Kittelson, D. B., and McMurry, P. H.: Structural properties of diesel exhaust particles measured by transmission electron microscopy (TEM): Relationships to particle mass and mobility, Aerosol Sci. Technol., 38, 881–889, https://doi.org/10.1080/027868290505189, 2004.

Pagels, J., Khalizov, A.F., McMurry, P.H. and Zhang, R.Y.: Processing of soot by controlled sulphuric acid and water condensation-mass and mobility relationship, Aerosol Sci. Technol., 43, 629–640, https://doi.org/10.1080/02786820902810685, 2009.

Peng, J. F., Hu, M., Guo, S., Du, Z. F., Zheng, J., Shang, D. J., Zamora, M., Zeng, L. M., Shao, M., Wu, Y. S., Zheng, J., Wang, Y., Glen, C., Collins, D., Molina, M., and Zhang, R. Y.: Markedly enhanced absorption, and direct radiative forcing of black carbon under polluted urban environments, P. Natl. Acad. Sci. USA, 113(16), 4266–4271, https://doi.org/10.1073/pnas.1602310113, 2016.

Petters, M. D. and Kreidenweis, S. M.: A single parameter representation of hygroscopic growth and cloud condensation nucleus activity, Atmos. Chem. Phys., 7, 1961–1971, https://doi.org/10.5194/acp-7-1961-2007, 2007.

Paatero, P. and Tapper, U.: Positive matrix factorization: A nonnegative factormodel with optimal utilization of error estimates of data values, Environmetrics, 5, 111–126, 1994.

Peng, J. F., Hu, M., Guo, S., Du, Z. F., Zheng, J., M., Zeng, L. M., Shao, M., Wu, Y. S., Collins, D., Molina, M., and Zhang, R. Y.: Ageing and hygroscopicity variation of black carbon particles in Beijing measured by a quasi-atmospheric aerosol evolution

study (QUALITY) chamber, Atmos. Chem. Phys., 17(17), 10333-10348, https://doi.org/10.5194/acp-17-10333-2017, 2017.

Pan, X.L., Kanaya, Y., Taketani, F., Miyakawa, T., Inomata, S., Komazaki, Y., et al.: Emission characteristics of refractory black carbon aerosols from fresh biomass burning: a perspective from laboratory experiments, Atmos. Chem. Phys., 17(21), 13001–13016, https://doi.org/10.5194/acp-17-13001-2017, 2017.

Park, K., Cao, F., Kittelson, D. B., & McMurry, P. H.: Relationship between particle mass and mobility for diesel exhaust particles, Environ. Sci. Tehnol., 37, 577–583, https://doi.org/10.1021/es025960v, 2003.

Qiao, K., Wu, Z., Pei, X., Liu, Q., Shang, D., Zheng, J., Du, Z., Zhu,W.,Wu, Y., Lou, S., Guo, S., Chan, C.K., Pathak, R.K., Hallquist, M., Hu, M.: Size-resolved effective density of submicron particles during summertime in the rural atmosphere of Beijing. China, J. Environ. Sci. (China) 73, 69–77. https://doi.org/10.1016/j.jes.2018.01.012, 2018.

Rissler, J., Nordin, E. Z., Eriksson, A. C., Nilsson, P. T., Frosch, M., Sporre, M. K., Wierzbicka, A., Svenningsson, B., Londahl, J., Messing, M. E., Sjogren, S., Hemmingsen, J. G., Loft, S., Pagels, J. H., and Swietlicki, E.: Effective Density and Mixing State of Aerosol Particles in a Near-Traffic Urban Environment, Environ. Sci. Technol., 48, 6300–6308, https://doi.org/10.1021/es5000353, 2014.

Riemer, N., Vogel, H., and Vogel, B.: Soot aging time scales in polluted regions during day and night, Atmos. Chem. Phys., 4, 1885–1893, https://doi.org/10.5194/acp-4-1885-2004, 2004.

Ramanathan, V. and Carmichael, G.: Global and regional climate changes due to black carbon, Nat. Geosci., 36, 221-227, https://doi.org/10.1038/ngeo156, 2008.

Ren, J., Zhang, F., Wang, Y., Collins, D., Fan, X., Jin, X., et al.: Using different assumptions of aerosol mixing state and chemical composition to predict CCN concentrations based on field measurements in urban Beijing, Atmos. Chem. Phys., 18, 6907–6921, https://doi.org/10.5194/acp-18-6907-2018, 2018.

Rader, D.J., McMurry, P.H.: Application of the tandem differential mobility analyzer to studies of droplet growth or evaporation, J. Geophys. Res.- Atmos., 17, 771-787, https://doi.org/10.1016/0021-8502(86)90031-5, 1986.

Reyes-Villegas, E., Bannan, T., Le Breton, M., Mehra, A., Priestley, M., Percival, C., Coe, H., and Allan, J. D.: Online Chemical Characterization of Food-Cooking Organic Aerosols: Implications for Source Apportionment, Environ. Sci. Technol., 52, 5308–5318, https://doi.org/10.1021/acs.est.7b06278, 2018.

Schwarz, J. P., Gao, R. S., Spackman, J. R., Watts, L. A., Thomson, D. S., Fahey, D. W., Ryerson, T. B., Peischl, J., Holloway, J. S., Trainer, M., Frost, G. J., Baynard, T., Lack, D. A., de Gouw, J. A., Warneke, C., and Del Negro, L. A.: Measurement of the mixing state, mass, and optical size of individual black carbon particles in urban and biomass burning emissions, Geophys. Res. Lett., 35, L13810, https://doi.org/10.1029/2008GL033968, 2008.

Stokes, R. and Robinson, R.: Interactions in aqueous nonelectrolyte solutions, I. Solute-solvent equilibria, J. Phys. Chem.-US, 70, 2126–2131, 1966.

Sun, Y., Du, W., Fu, P., Wang, Q., Li, J., Ge, X., Zhang, Q., Zhu, C., Ren, L., Xu, W.,

Zhao, J., Han, T., Worsnop, D. R., and Wang, Z.: Primary, and secondary aerosols in Beijing in winter: sources, variations, and processes, Atmos. Chem. Phys., 16, 8309–8329, https://doi.org/10.5194/acp-16-8309-2016,2016.

Sun, Y. L., Wang, Z. F., Du, W., Zhang, Q., Wang, Q. Q., Fu, P. Q., Pan, X. L., Li, J., Jayne, J., and Worsnop, D. R.: Long term real-time measurements of aerosol particle composition in Beijing, China: seasonal variations, meteorological effects, and source analysis, Atmos. Chem. Phys., 15, 10149–10165, https://doi.org/10.5194/acp-15-10149-2015, 2015.

Shiraiwa, M., Kondo, Y., Moteki, N., Takegawa, N., Sahu, L., Takami, A., et al.: Radiative impact of mixing state of black carbon aerosol in Asian outflow, J. Geophys. Res.- Atmos., 113, D24210, https://doi.org/ 10.1029/2008JD010546, 2008.

Tan, H., Xu, H., Wan, Q., Li, F., Deng, X., Chan, P. W., Xia, D., and Yin, Y.: Design and application of an unattended multifunctional H-TDMA system, J. Atmos. Ocean. Tech., 30, 1136–1148, https://doi.org/10.1175/JTECH-D-12-00129.1, 2013.

Ulbrich, I. M., Canagaratna, M. R., Zhang, Q., Worsnop, D. R., and Jimenez, J. L.: Interpretation of organic components from Positive Matrix Factorization of aerosol mass spectrometric data, Atmos. Chem. Phys., 9, 2891–2918, https://doi.org/10.5194/acp-9- 2891-2009, 2009.

Wang, Y., Wan, Q., Meng, W., Liao, F., Tan, H., and Zhang, R.: Long-term impacts of aerosols on precipitation and lightning over the Pearl River Delta megacity area in China, Atmos. Chem. Phys., 11, 12421–12436, https://doi.org/10.5194/acp-11-12421-2011, 2011.

Wang, Y. Y., Liu, F. S., He, C. L., Bi, L., Cheng, T. H., Wang, Z. L., Zhang, H., Zhang, X. Y., Shi, Z. B., and Li, W. J.: Fractal dimensions and mixing structures of soot particles during atmospheric processing, Environ. Sci. Tech. Lett., 4, 487–493, https://doi.org/10.1021/acs.estlett.7b00418, 2017.

Wu, Y. F., Xia, Y. J., Huang, R. J., Deng, Z. Z., Tian, P., Xia, X. G., et al.: A study of the morphology and effective density of externally mixed black carbon aerosols in ambient air using a size-resolved single-particle soot photometer (SP2), Atmos. Meas. Tech., 12, 4347–4359, https://doi.org/10.5194/amt-12-4347-2019, 2019.

Wu, Y., Wang, X., Tao, J., Huang, R., Tian, P., Cao, J., Zhang, L., Ho, K.-F., Han, Z., and Zhang, R.: Size distribution and source of black carbon aerosol in urban Beijing during winter haze episodes, Atmos. Chem. Phys., 17, 7965–7975, https://doi.org/10.5194/acp-17-7965-2017, 2017.

Wu, Z. J., Zheng, J., Shang, D. J., Du, Z. F., Wu, Y. S., Zeng, L. M., Wiedensohler, A., and Hu, M.: Particle hygroscopicity and its link to chemical composition in the urban atmosphere of Beijing, China, during summertime, Atmos. Chem. Phys., 16, 1123–1138, https://doi.org/10.5194/acp-16-1123-2016, 2016.

Xue, H., Khalizov, A. F., Wang, L., Zheng, J., and Zhang, R.: Effects of dicarboxylic acid coating on the optical properties of soot, Phys. Chem. Chem. Phys., 11, 7869–7875, https://doi.org/10.1039/b904129j, 2009.

Xu, W., Sun, Y., Wang, Q., Zhao, J., Wang, J., Ge, X., et al.: Changes in aerosol chemistry from 2014 to 2016 in winter in beijing: Insights from high-resolution aerosol mass spectrometry, J. Geophys. Res.-Atmos., 124, 1132–1147.

814   https://doi.org/10.1029/2018jd029245, 2019.

815 Xu, W., Fossum, K. N., Ovadnevaite, J., Lin, C., Huang, R.-J., O'Dowd, C., and
816   Ceburnis, D.: The impact of aerosol size-dependent hygroscopicity and mixing state
817   on the cloud condensation nuclei potential over the north-east Atlantic, Atmos. Chem.
818   Phys., 21, 8655–8675, https://doi.org/10.5194/acp-21-8655-2021, 2021.

819 Yuan, T., Li, Z., Zhang, R., and Fan, J.: Increase of cloud droplet size with aerosol
820   optical depth: An observation and modeling study, J. Geophys. Res.-Atmos., 113,
821   D04201, https://doi.org/10.1029/2007JD008632, 2008.

822 Yu, C., Liu, D., Broda, K., Joshi, R., Olfert, J., Sun, Y., Fu, P., Coe, H., Allan, J.D.:
823   Characterising mass-resolved mixing state of black carbon in Beijing using a
824   morphology-independent measurement method, Atmos. Chem. Phys., 20, 3645–
825   3661. https://doi.org/10.5194/acp-20-3645-2020, 2020.

826 Zhang, R. Y., Khalizov, A. F., Pagels, J., Zhang, D., Xue, H. X., and McMurry, P. H.:
827   Variability in morphology, hygroscopicity, and optical properties of soot aerosols
828   during atmospheric processing, P. Natl. Acad. Sci. USA, 105, 10291–10296,
829   https://doi.org/10.1073/pnas.0804860105, 2008.

830 Zhang, Y., Zhang, Q., Cheng, Y., Su, H., Kecorius, S., Wang, Z., Wu, Z., Hu, M., Zhu,
831   T., Wiedensohler, A., and He, K.: Measuring the morphology and density of
832   internally mixed black carbon with SP2 and VTDMA: new insight into the
833   absorption enhancement of black carbon in the atmosphere, Atmos. Meas. Tech., 9,
834   1833–1843, https://doi.org/10.5194/amt-9-1833-2016, 2016.

835 Zdanovskii, A.: New methods for calculating solubilities of electrolytes in
836   multicomponent systems, Zh. Fiz. Khim.C, 22, 1475– 1485, 1948.

837 Zhang, F., Wang, Y., Peng, J., Ren, J., Collins, D., Zhang, R., et al.: Uncertainty in
838   predicting CCN activity of aged and primary aerosols, J. Geophys. Res.-Atmos.,
839   122(21), 11723–11736, https://doi.org/10.1002/2017jd027058, 2017.

840 Zhang, F., Ren, J., Fan, T., Chen, L., Xu, W., Sun, Y., et al.: Significantly enhanced
841   aerosol CCN activity and number, J. Geophys. Res.-Atmos., 124, 14102–14113,
842   https://doi.org/10.1029/2019jd031457, 2019.

843 Zhang, F., Wang, Y., Peng, J., Chen, L., Sun, Y., Duan, L., Ge, X., Li, Y., Zhao, J., Liu,
844   C., Zhang, X., Zhang, G., Pan, Y., Wang, Y., Zhang, A. L., Ji, Y., Wang, G., Hu, M.,
845   Molina, M. J., Zhang, R.: An unexpected catalyst dominates formation and radiative
846   forcing of regional haze, P. Natl. Acad. Sci. USA, 117(8), 3960-3966,
847   https://doi.org/10.1073/pnas.1919343117, 2020a.

848 Zhang, Y., Zhang, Q., Yao, Z., Li, H.: Particle Size and Mixing State of Freshly Emitted
849   Black Carbon from Different Combustion Sources in China, Environ. Sci. Technol.,
850   54(13): p. 7766-7774, https://doi.org/10.1021/acs.est.9b07373, 2020b.

851 Zhang, F., Peng, J., Chen, L., Collins, D., Li, Y., Jiang, S., Liu, J., Zhang, R.: The effect
852   of Black carbon aging from NO2 oxidation of SO2 on its morphology, optical and
853   hygroscopic properties, Environ. Res., 212, 113238,
854   https://doi.org/10.1016/j.envres.2022.113238, 2022.

855 Zhang, R., Wang, G., Guo, S., Zamora, M. L., Ying, Q., Lin, Y.: Formation of urban
856   fine particulate matter, Chemical Reviews, 115(10), 3803–3855,
857   https://doi.org/10.1021/acs.chemrev.5b00067, 2015.

858 Zhou, Y., Ma, N., Wang, Q., Wang, Z., Chen, C., Tao, J., Hong, J., Peng, L., He, Y.,

859 Xie, L., Zhu, S., Zhang, Y., Li, G., Xu, W., et al.: Bimodal distribution of size-
860 resolved particle effective density: results from a short campaign in a rural environ
861 ment over the North China Plain, Atmos. Chem. Phys., 22, 2029–2047.
862 https://doi.org/10.5194/acp-22-2029-2022, 2022.

863 Zhao, G., Tan, T., Hu, S., Du, Z., Shang, D., Wu, Z., Guo, S., Zheng, J., Zhu, W., Li,
864 M., Zeng, L., and Hu, M.: Mixing state of black carbon at different atmospheres in
865 north and southwest China, Atmos. Chem. Phys., 22, 10861–10873,
866 https://doi.org/10.5194/acp-22-10861-2022, 2022.